JOURNAL OF GUIDANCE, CONTROL, AND DYNAMICS
Vol. 27, No. 1, January–February 2004

Gain–Phase Margin Analysis of Pilot-Induced Oscillations for Limit-Cycle Prediction

Bing-Fei Wu* and Jau-Woei Perng†
National Chiao Tung University, Hsinchu 300, Taiwan, Republic of China

This investigation attempts to forecast the limit cycles of pilot-induced oscillations (PIOs) by combining the gain-phase margin tester, the M-locus, and the parameter plane methods. First, one position- or rate-limited nonlinear element is linearized by the conventional means of describing functions. The stability of an equivalent linearized system with adjustable parameters is then analyzed using stability equations and the parameter plane method. Additionally, the minimum gain-phase margin of the PIO system at which a limit cycle can occur is determined by inserting the gain-phase margin tester into the forward open-loop system. Moreover, a simple method is developed to identify the intersections of the M locus and the constant gain and phase boundaries in the parameter plane. In so doing the exact relationship between the gain–phase margin and the characteristics of the limit cycle can be clearly determined. The results of this study demonstrate that these procedures can enhance the analysis of PIO over analysis by other methods in the literature. This approach is extended to PIO analysis with multiple nonlinearities.

I. Introduction

PILOT-INDUCED oscillations (PIOs), which are due to complex interactions between a pilot and an aircraft, have been researched over recent years.[1–7] The generation of PIOs that include one or more hard nonlinearities frequently causes a large variation in the amplitude, which is dangerous to aircraft. Therefore, predicting limit cycles is very important in preventing worst-case PIOs. The traditional method of analyzing the amplitude and frequency of a limit cycle is to linearize the nonlinear elements according to the describing function method.[8,9] Uncertain parameters in a linear control system can be robustly analyzed by the parameter plane method or the parameter space method.[10–15] Based on the M-locus method, the describing function of nonlinearities can be represented in the parameter plane or parameter space to elucidate the characteristics of limit cycles.[16]

A designer must carefully consider the range of safe operation of a system because varying parameters and phase lag always impact practical control systems. Gain margin (GM) and phase margin (PM) are two important specifications in the analysis and design of practical control systems. Methods of analyzing the gain–phase margin of a linear control system with adjustable parameters have recently been developed.[17,18] The approach in Ref. 17 has been extended to analyze a nuclear reactor system with several transport lags.[19] Thereafter, Refs. 20–23 addressed the prediction of limit cycles in nonlinear control systems such as a reactor system, a low-flying vehicle, and a gun turret. Moreover, the control parameters of an engine system can be determined by describing function and parameter space approaches to yield the specific amplitude and frequency of the limit cycle to meet system requirements.[24]

This work describes a systematic strategy for analyzing the limit cycles of PIOs caused by the variation of parameters and hard nonlinearities. A simple method is also presented to evaluate the gain–phase margins and the M locus in the parameter plane to measure stability after a gain–phase margin tester is added to the forward open loop of a linearized control system. The proposed approach greatly facilitates the implementation of the nonlinear control system design and yields more information on limit cycles than provided by other studies.[3–7] Finally, two examples of PIO in the current literature[3,4] are offered to illustrate the design procedures.

The paper is organized as follows: Section II outlines the basic approach. Section III presents the first example of X-15 PIO with one nonlinear element to demonstrate the design procedures. Section IV extends the approach to analyze YF-12 PIO with multiple nonlinearities. Finally, Section V draws conclusions.

II. Basic Approach

A general nonlinear control system including m nonlinearities $(n_1, n_2, \ldots, n_m)$ is considered. The nonlinear control system may be approximately linearized by the classical describing function method. Figure 1 depicts the linearized system with a gain–phase margin tester $(Ke^{-j\theta})$ inserted in the forward open-loop system, where $G(s, N_{1R}, N_{1I}, \ldots, N_{mR}, N_{mI})$ is the open-loop transfer function. The terms $N_{1R}, \ldots, N_{mR}$ and $N_{1I}, \ldots, N_{mI}$ are the real and imaginary parts of the describing function (N_i) of $n_1, n_2, \ldots, n_m$, respectively. The function can be expressed as follows:

$$N_i(A, \omega) = N_{iR}(A, \omega) + jN_{iI}(A, \omega), \qquad i = 1, \ldots, m \quad (1)$$

where A and ω are the amplitude and frequency of a sinusoidal input to one of the nonlinearities. The characteristic equation of this equivalent linear system is

$$1 + Ke^{-j\theta}G(s, N_{1R}, N_{1I}, \ldots, N_{mR}, \ldots, N_{mI}) = 1 + Ke^{-j\theta}\frac{N(s, N_{1R}, N_{1I}, \ldots, N_{mR}, \ldots, N_{mI})}{D(s, N_{1R}, N_{1I}, \ldots, N_{mR}, \ldots, N_{mI})} = 0 \quad (2)$$

which is equivalent to

$$f(s) \triangleq D(s, N_{1R}, N_{1I}, \ldots, N_{mR}, \ldots, N_{mI}) + ke^{-j\theta}N(s, N_{1R}, N_{1I}, \ldots, N_{mR}, \ldots, N_{mI}) = 0 \quad (3)$$

Let $s = j\omega$, such that

$$f(j\omega) = f(\alpha, \beta, \gamma, \ldots, K, \theta, j\omega) = 0 \quad (4)$$

Received 28 October 2002; revision received 25 March 2003; accepted for publication 4 August 2003.

*Professor, Department of Electrical and Control Engineering, 1001 Ta Hsueh Road; bwu@cc.nctu.edu.tw.

†Research Assistant Professor, Department of Electrical and Control Engineering, 1001 Ta Hsueh Road.

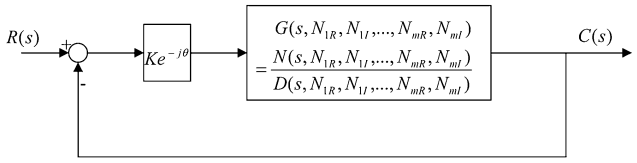

Fig. 1 Block diagram of a linearized nonlinear control system with a gain–phase margin tester.

where $\alpha, \beta, \gamma, \ldots,$ are variables which consist of the items (N_{IR}, N_{iI}) of the describing functions and/or the adjustable parameters of the linear part of the system.[14,16] Notably, the designer can arbitrarily define these variables to analyze the effect of the system parameters. When only two parameters α and β are considered, Eq. (4) is arranged as follows:

$$f(j\omega) = f(\alpha, \beta, \gamma, \ldots, K, \theta, j\omega) = X \cdot \alpha + Y \cdot \beta + Z = 0 \quad (5)$$

where X, Y, and Z are functions of $\gamma, \ldots, K, \theta$ and $j\omega$. Let Eq. (5) be partitioned into two stability equations with a real part f_R and an imaginary part f_I, written as

$$f_R(\alpha, \beta, \gamma, \ldots, K, \theta, \omega) = X_1 \cdot \alpha + Y_1 \cdot \beta + Z_1 = 0 \quad (6)$$

$$f_I(\alpha, \beta, \gamma, \ldots, K, \theta, \omega) = X_2 \cdot \alpha + Y_2 \cdot \beta + Z_2 = 0 \quad (7)$$

where X_1, Y_1, Z_1 and X_2, Y_2, Z_2 are real and imaginary parts of X, Y, and Z. Consequently, α and β are determined from the linear functions of Eqs. (6) and (7),

$$\alpha = (Y_1 \cdot Z_2 - Y_2 \cdot Z_1)/\Delta \quad (8)$$

$$\beta = (Z_1 \cdot X_2 - Z_2 \cdot X_1)/\Delta \quad (9)$$

where $\Delta = (X_1 \cdot Y_2 - X_2 \cdot Y_1)$. Notably, if Eqs. (6) and (7) are not linear, but independent of α and β, then they can be solved analytically.[16]

Let $K = 0$ dB and $\theta = 0$ deg, and set the remaining variables $(\gamma, \ldots,)$ equal to constants. Then, for various values of ω, a locus called the stability boundary of the system without the gain–phase margin tester can be plotted in the α–β. If K is assumed to be equal to another constant and $\theta = 0$ deg, then the locus in the α–β plane is a boundary of the constant GM. However, if $K = 0$ dB and θ is assumed to be equal to another constant, then the locus is a boundary of the constant PM.[17,19] Additionally, when the third parameter γ is considered, the three aforementioned boundaries can be also found in parameter space for each specific value of γ.[9,10]

The describing function with one nonlinearity can be represented by an M locus in the parameter plane to analyze the limit-cycle properties of the nonlinear control system in Ref. 16. The M-locus method[20,21] related to the GM for asymptotic stability and dependent on A, ω, and K is called M_{GM} and that related to the PM for asymptotic stability and dependent on A, ω, and θ is called M_{PM}. The term M_{GM} equals M_{PM} when the describing functions of the nonlinearities depend on amplitude but not on frequency. However, the loci are unequal when the describing functions depend on both amplitude and frequency.

The relative locations of the stability boundary, the M_{GM} locus and the M_{PM} locus, can be used to establish the existence and stability of limit cycles by examining the intersections of the stability boundary and the describing curve and the direction of increasing A, respectively.[20,21] After the boundaries of constant GM and PM have been plotted, the GM and the PM at the intersections of these boundaries and the M_{GM} and M_{PM} loci can be determined. Moreover, the GM and the PM can both be plotted against A. GM_{min} and PM_{min}, defined as the minimum values of GM and PM, represent the minimum amounts by which the loop gain and phase shift must be increased or decreased to produce or eliminate a limit-cycle solution.

A brief method for obtaining the GM and PM and plotting the loci of M_{GM} and M_{PM} in the parameter plane is proposed to simplify the aforementioned procedures. Let $\theta = 0$ deg; Eq. (4) is rearranged as follows:

$$f(j\omega) = f(\alpha, \beta, \gamma, \ldots, K, j\omega) = E \cdot K + F = 0 \quad (10)$$

Partitioning Eq. (10) into real and imaginary parts yields

$$f_R(\alpha, \beta, \gamma, \ldots, K, \omega) = E_1 \cdot K + F_1 = 0 \quad (11)$$

$$f_I(\alpha, \beta, \gamma, \ldots, K, \omega) = E_2 \cdot K + F_2 = 0 \quad (12)$$

where E_1, E_2, F_1, and F_2 are functions of $\alpha, \beta, \gamma, \ldots, \omega$. Thus, K can be determined directly from Eqs. (11) and (12), which yield

$$K = (-F_1/E_1) \triangleq K' \quad (13)$$

$$K = (-F_2/E_2) \triangleq K'' \quad (14)$$

If $K' = K'' = K_i$ for $A = A_i$, the values of A_i and K_i related to ω_i can be found by varying A from 0 to ∞. For many values of ω, a set (GM) of desired values of A and K can be obtained and connected as the M_{GM} locus in the parameter plane. Alternately, let $K = 0$ dB; Eq. (4) is rearranged as follows:

$$f(j\omega) = f(\alpha, \beta, \gamma, \ldots, \theta, j\omega) = U \cdot \cos\theta + V \cdot \sin\theta + W = 0 \quad (15)$$

Also, partitioning Eq. (15) into real and imaginary parts yields

$$f_R(\alpha, \beta, \gamma, \ldots, \theta, \omega) = U_1 \cdot \cos\theta + V_1 \cdot \sin\theta + W_1 = 0 \quad (16)$$

$$f_I(\alpha, \beta, \gamma, \ldots, \theta, \omega) = U_2 \cdot \cos\theta + V_2 \cdot \sin\theta + W_2 = 0 \quad (17)$$

where U_1, V_1, W_1, U_2, V_2, and W_2 are functions of $\alpha, \beta, \gamma, \ldots, \omega$. Hence, θ can be determined directly from Eqs. (16) and (17), which yield

$$\theta = \cos^{-1}\left(\frac{V_1 \cdot W_2 - V_2 \cdot W_1}{U_1 \cdot V_2 - U_2 \cdot V_1}\right) \triangleq \theta' \quad (18)$$

$$\theta = \sin^{-1}\left(\frac{U_1 \cdot W_2 - U_2 \cdot W_1}{U_1 \cdot V_2 - U_2 \cdot V_1}\right) \triangleq \theta'' \quad (19)$$

If $\theta' = \theta'' = \theta_i$ for $A = A_i$, A_i, and θ_i related to ω_i can be found by varying A from 0 to ∞. For many values of ω, a set (PM) of desired values for A and θ can be obtained and connected as the M_{PM} locus in the parameter plane.

III. Case 1: Pilot-Induced Oscillation Analysis of X-15 (with One Nonlinearity)

This section considers the PIO of X-15,[1] which has only one nonlinear element of a rate-limited actuator. Figure 2 shows the

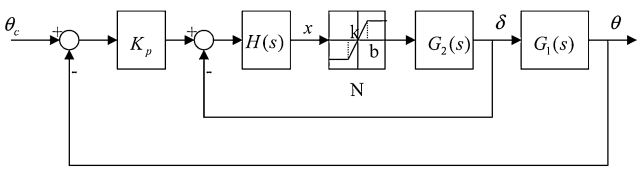

Fig. 2 Block diagram of the X-15 pilot–vehicle system.

block diagram of this system. The following numerical data are adopted[3]:

$$G_1(s) = \frac{\theta(s)}{\delta(s)} = \frac{3.476(s+0.0292)(s+0.883)}{(s^2+0.019s+0.01)(s^2+0.8418s+5.29)} \tag{20}$$

$$G_2(s) = \frac{1}{s} \tag{21}$$

$$H(s) = 25 \tag{22}$$

The nonlinear element N represents the rate-limited actuator. Assume that the signal input to N is $x(t) = A\sin\omega t$; the describing function of N is as follows[8,9]:

$$N(A) = (2k/\pi)\left[\sin^{-1}(b/A) + (b/A)(1-b^2/A^2)^{\frac{1}{2}}\right] \qquad A > b \tag{23}$$

where $k = 1$ and $b = 15$.

Remark 1: Because N depends on amplitude but not on frequency, only one M locus need be considered ($M_{GM} = M_{PM}$).

The overall open-loop transfer function is

$$G(s) = \frac{K_p H(s)N(A)G_1(s)G_2(s)}{1 + H(s)N(A)G_1(s)}$$

$$= \frac{86.9K_pN(A)(s+0.0292)(s+0.883)}{(s+25N(A))(s^2+0.019s+0.01)(s^2+0.8418s+5.29)} \tag{24}$$

When the gain–phase margin tester is cascaded to the open-loop system, the characteristic equation becomes

$$\begin{aligned} f(s) &= (s+25N(A))(s^2+0.019s+0.01)(s^2+0.8418s+5.29) \\ &\quad + Ke^{-j\theta}86.9K_pN(A)(s+0.0292)(s+0.883) \\ &= 86.9Ke^{-j\theta}(s+0.0292)(s+0.883)K_pN(A) \\ &\quad + 25(s^2+0.019s+0.01)(s^2+0.8418s+5.29)N(A) \\ &\quad + s(s^2+0.019s+0.01)(s^2+0.8418s+5.29) \\ &= X\cdot\alpha + Y\cdot\beta + Z = 0 \end{aligned} \tag{25}$$

where $\alpha = K_pN(A)$ and $\beta = N(A)$ are adjustable parameters. Substituting $s = j\omega$ into Eq. (25) enables α and β to be determined from Eqs. (6–9) by varying ω from 0 to ∞. Then, the stability boundary ($K = 0$ dB, $\theta = 0$ deg) can be plotted in the K_p vs $N(A)$ plane, where $K_p = \alpha/\beta$ and $N(A) = \beta$. Figure 3 shows the results.

In Ref. 3, the algorithm called ROBAN is employed to perform a robust stability analysis of a linear time-invariant system with uncertain parameters, where $N(A)$ is replaced by the linear time-invariant gain L within the range [0,1]. Importantly, the stability boundary in Fig. 3 is not the same as that in Ref. 3. Figure 4 shows the stability conditions of the linear system obtained from the time simulations of the unit step input signal with four test points ($K_p = 0.75$, 1.5, 2.23, 3, and $L = 1$). The output simulation results are also considered to check the accuracy of Fig. 3. The linear systems are stable when $K_p = 0.75$ and 1.5. However, the linear systems are marginally stable and unstable when $K_p = 2.23$ and 3, respectively. As an example for comparison, when $K_p = 3$ and $L = 1$, the stability condition in Ref. 3 is inconsistent with the results obtained here. Accordingly, the context of the robust stability analysis of the linear system and the limit-cycle analysis of the nonlinear system in Ref. 3 should be modified.

The limit-cycle analysis with one nonlinear element N of X-15 PIO can also be obtained from Fig. 3. The following three conditions apply:

1) For $K_p < 0.89$, no limit cycles exist.

2) For $0.89 \le K_p < 2.23$, two limit cycles exist. (One is stable and the other is unstable.)

3) For $2.23 \le K_p$, only one stable limit cycle exists.

The stability of limit cycles was addressed in Ref. 3. Based on the describing function method, the amplitude and the frequency of limit cycles can be clearly obtained from Fig. 5. Due to yield limit cycles, the slope of the nonlinear element may be reduced from one to zero (L is decreased) but K_p remains fixed. The nonlinear element

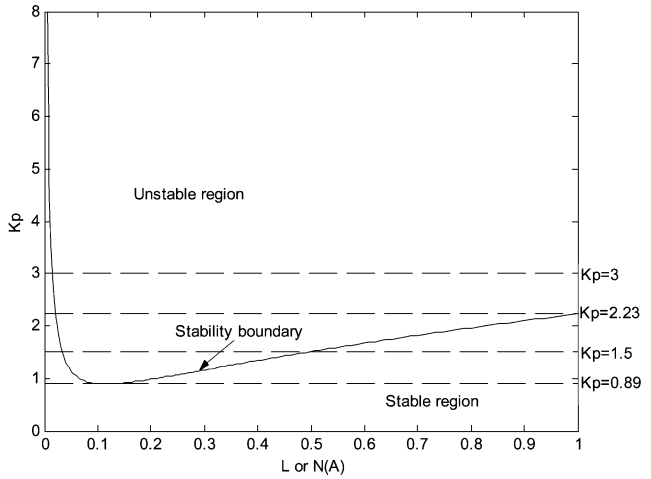

Fig. 3 Robust stability analysis of X-15 PIO.

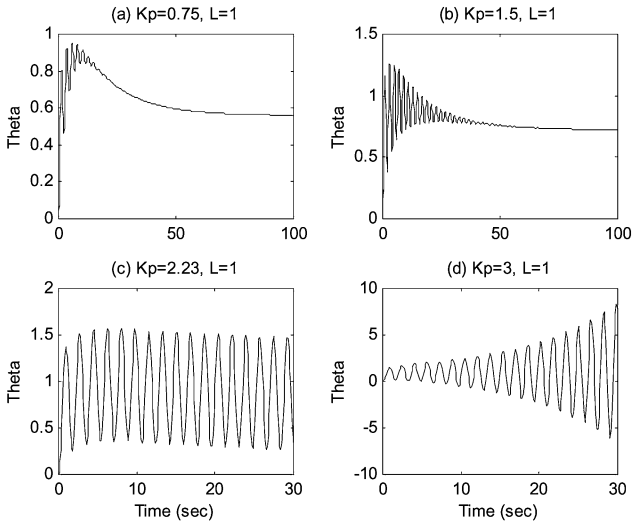

Fig. 4 Output simulation results of equivalent linear system.

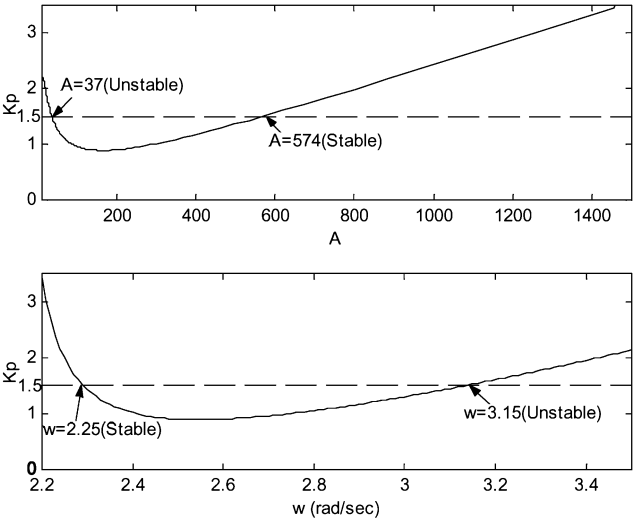

Fig. 5 Predication of amplitude and frequency of limit cycle with pilot gain.

is guaranteed to operate in the saturation region. Figure 6 presents the time simulation results at four test points ($K_p = 0.75$, 1.5, 2.23, 3), under the preceding three conditions.

Finally, the gain–phase margin analysis of the nonlinear system is considered. Let $\theta = 0$ deg; Eq. (25) is rearranged as follows:

$$f(s) = 86.9K_pN(A)(s + 0.0292)(s + 0.883)K + (s + 25N(A))(s^2 + 0.019s + 0.01)(s^2 + 0.8418s + 5.29) = E \cdot K + F = 0 \quad (26)$$

Substituting $s = j\omega$ into Eq. (26) and varying A from 0 to ∞ enables a set of A_i and K_i, related to ω_i, to be obtained directly from Eqs. (11–14). Alternatively, let $K = 0$ dB; Eq. (25) is rearranged as follows:

$$f(s) = 86.9K_pN(A)(s + 0.0292)(s + 0.883)\cos\theta + 86.9K_pN(A)(s + 0.0292)(s + 0.883)(-j)\sin\theta + (s + 25N(A))(s^2 + 0.019s + 0.01)(s^2 + 0.8418s + 5.29) = U \cdot \cos\theta + V \cdot \sin\theta + W = 0 \quad (27)$$

Substituting $s = j\omega$ into Eq. (27) and varying A from 0 to ∞ enables a set of A_i and θ_i, related to ω_i, to be directly obtained from Eqs. (16–19).

Based on the analysis in the preceding paragraph, Fig. 7 illustrates some M loci for different values of K_p and various boundaries of

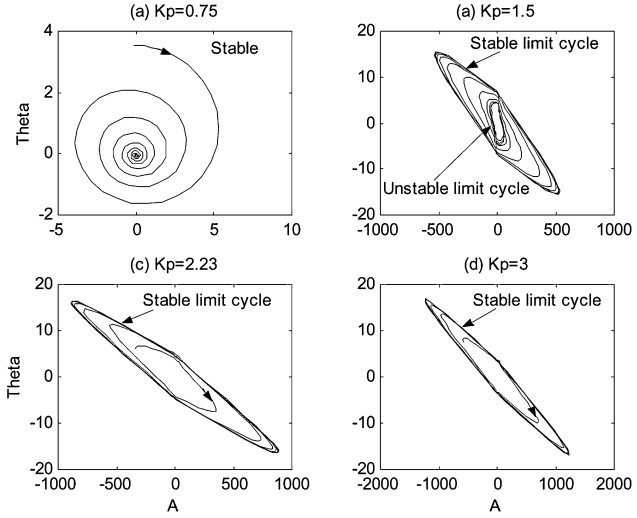

Fig. 6 Time simulations of limit cycles with different pilot gains.

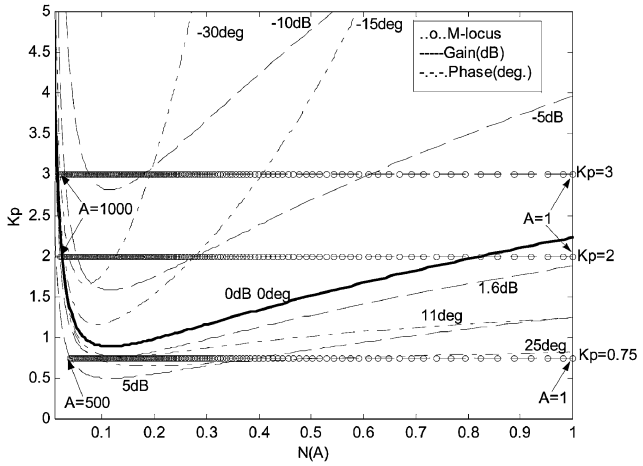

Fig. 7 M loci and boundaries of constant gain–phase margin in the parameter plane.

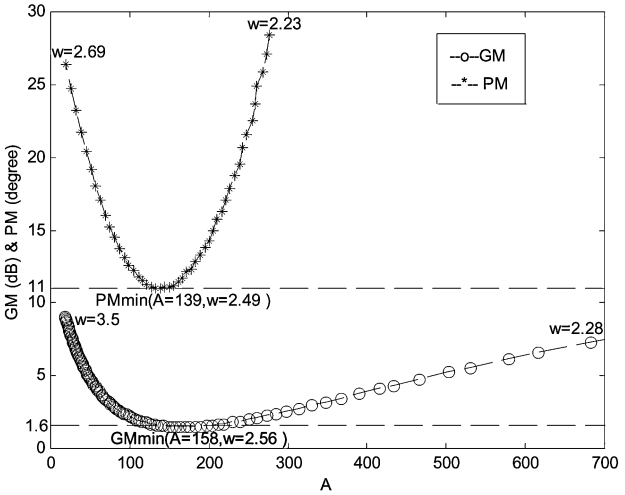

Fig. 8 The intersection points between M loci and boundaries of constant gain–phase margin with pilot gain $K_p = 0.75$.

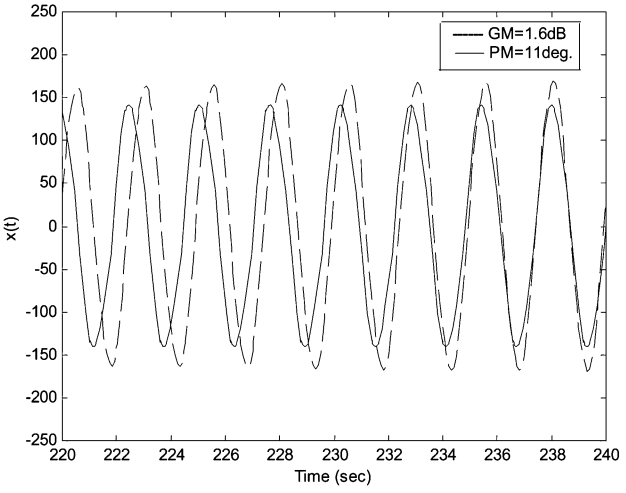

Fig. 9 Simulation result of limit cycles with increased gain and phase.

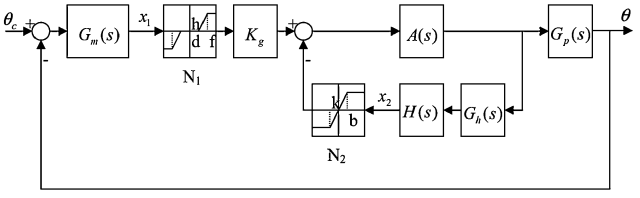

Fig. 10 Block diagram of YF-12 pilot–vehicle system.

constant gain (K) and constant phase (θ). If $K_p = 0.75$ (stable) is set, the margins of gain and phase associated with the limit cycle are obtained from Fig. 8. Therefore, two curves ($GM_{min} = 1.6$ dB and $PM_{min} = 11$ deg) are tangent to the M locus and produce the limit cycle. The amplitude and frequency of the limit cycles at other values of GM (K) and PM (θ) can be obtained directly from Fig. 8. Figure 9 shows the time responses of the limit cycle obtained by adding $K = 1.6$ dB and $\theta = 11$ deg. The simulation results in Figs. 8 and 9 are observed to be consistent.

IV. Case 2: Pilot-Induced Oscillation Analysis of YF-12 (with Multiple Nonlinearities)

This section considers PIO analysis with multiple nonlinearities of YF-12.[2] Figure 10 presents the related block diagram. The

following numerical data are adopted[4]:

$$G_m(s) = \frac{K_p}{T_n s + 1} \tag{28}$$

$$G_p(s) = \frac{11.17s^3 + 21.975s^2 + 1504.216s + 1180.8}{s^5 + 3.07s^4 + 252.355s^3 + 375.28s^2 + 984s} \tag{29}$$

$$G_h(s) = \frac{6(s + 0.8)}{(s^2 + 1.5s + 4)} \tag{30}$$

$$A(s) = \frac{34}{(s + 34)} \tag{31}$$

$$H(s) = \frac{0.375(s + 8)}{(s + 4)} \tag{32}$$

$$K_g = 0.74 \tag{33}$$

The first nonlinear element, N_1, represents the breakout and the control-stick travel limiter. The second nonlinear element, N_2, models the stability augmentation system limiter. Assume that the input signals to N_1 and N_2 are $x_1(t) = A_1 \sin \omega t$, and $x_2(t) = A_2 \sin \omega t$, respectively. The describing functions of N_1 and N_2 are as follows[8,9]:

$$N_1(A_1) = \frac{2h}{\pi}\left(\sin^{-1}\frac{f}{A_1} - \sin^{-1}\frac{d}{A_1} + \frac{f}{A_1}\left(1 - \frac{f^2}{A_1^2}\right)^{\frac{1}{2}} - \frac{d}{A_1}\left(1 - \frac{d^2}{A_1^2}\right)^{\frac{1}{2}}\right), \qquad A_1 > f \tag{34}$$

$$N_2(A_2) = \frac{2k}{\pi}\left(\sin^{-1}\frac{b}{A_2} + \frac{b}{A_2}\left(1 - \frac{b^2}{A_2^2}\right)^{\frac{1}{2}}\right), \qquad A_2 > b \tag{35}$$

where, $h = 0.5$, $d = 5$, $f = 25$, $k = 1$, and $b = 2.5$.

Remark 2: $x_2(t)$ is selected as the reference input signal for analysis, then A_1 can be expressed as a function of A_2 and ω, $A_1(A_2, \omega)$, so that N_1 depends on amplitude and frequency when A_2 and ω are known, implying that M_{GM} and M_{PM} must be considered, respectively.[20,21]

The overall open-loop transfer function is

$$G(s) = \frac{G_m(s)A(s)N_1(A_1)K_g G_p(s)}{1 + A(s)G_h(s)H(s)N_2(A_2)} = \frac{34K_p N_1(A_1)K_g(s + 4)(s^2 + 1.5s + 4)(11.17s^3 + 21.98s^2 + 1504.22s + 1180.8)}{(T_n s + 1)(s^5 + 3.07s^4 + 252.36s^3 + 375.28s^2 + 984s) \times \left[(s + 4)(s + 34)(s^2 + 1.5s + 4) + 76.5(s + 0.8)(s + 8)N_2(A_2)\right]} \tag{36}$$

When the gain–phase margin tester is cascaded to the open-loop system, the characteristic equation becomes

$$\begin{aligned} f(s) = {} & (T_n s + 1)(s^5 + 3.07s^4 + 252.36s^3 + 375.28s^2 + 984s) \\ & \times \left[(s + 4)(s + 34)(s^2 + 1.5s + 4) + 76.5(s + 0.8)\right. \\ & \left. \times (s + 8)N_2(A_2)\right] + Ke^{-j\theta}34K_p N_1(A_1)K_g(s + 4) \\ & \times (s^2 + 1.5s + 4)(11.17s^3 + 21.98s^2 \\ & + 1504.22s + 1180.8) = 0 \end{aligned} \tag{37}$$

First, the two adjustable parameters $\alpha = K_p$ and $\beta = T_n$ can be plotted by the boundaries with fixed amplitude A_2 (varying ω from 0 to ∞) and fixed frequency ω (varying A_2 from 0 to ∞) in the K_p vs T_n plane, as shown in Fig. 11. These boundaries distinguish two regions, one of which is the asymptotically stable region and the other of which is the limit-cycle region. Four curves ($A_2 = 3.78$, $A_2 = 10.4$, $\omega = 3.9$, and $\omega = 5.04$) pass through Q_1 (limit cycle region: $K_p = 20, T_n = 0.15$),[4] and two limit cycles can be determined:

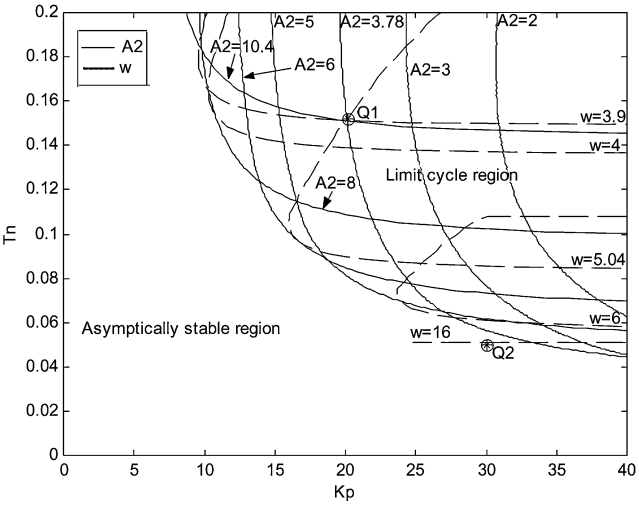

Fig. 11 Limit-cycle loci in parameter plane.

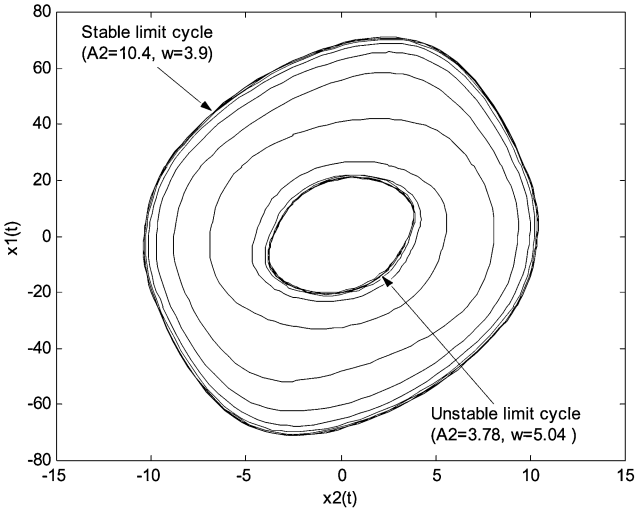

Fig. 12 Simulation results of two limit cycles.

1) a stable limit cycle ($A_2 = 10.4$, $\omega = 3.9$) and 2) an unstable limit cycle ($A_2 = 3.78$, $\omega = 5.04$). Figure 12 shows the time simulations of these two limit cycles. If another point, Q_2 ($K_p = 30$, $T_n = 0.05$), is selected from Fig. 11, a high-frequency (16 rad/s) limit cycle is obtained, for which the result was also discussed in Ref. 4.

Second, two parameters, $\alpha = N_1(A_1)$ and $\beta = N_2(A_2)$, are determined following the aforementioned procedures. Hence, the stability boundary ($K = 0$ dB, $\theta = 0$ deg) of Q_1 ($K_p = 20$, $T_n = 0.15$) can be determined in the N_1 vs N_2 plane and is represented as a thick solid line in Fig. 13.

Finally, the gain–phase margin analysis of the nonlinear system is considered. Rearranging Eq. (37) again, and letting $\theta = 0$ deg, yields

$$\begin{aligned} f(s) = {} & 34K_p N_1(A_1)K_g(s + 4)(s^2 + 1.5s + 4)(11.17s^3 + 21.98s^2 \\ & + 1504.22s + 1180.8)K + (T_n s + 1)(s^5 + 3.07s^4 + 252.36s^3 \\ & + 375.28s^2 + 984s)\left[(s + 4)(s + 34)(s^2 + 1.5s + 4)\right. \\ & \left. + 76.5(s + 0.8)(s + 8)N_2(A_2)\right] = E \cdot K + F = 0 \end{aligned} \tag{38}$$

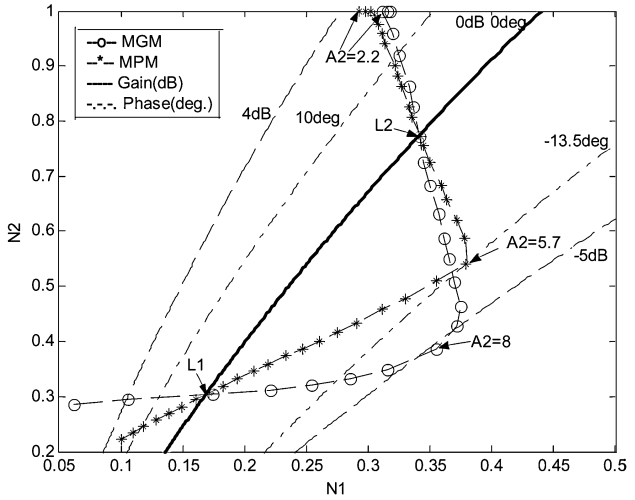

Fig. 13 M loci and boundaries of constant gain–phase margin in the parameter plane.

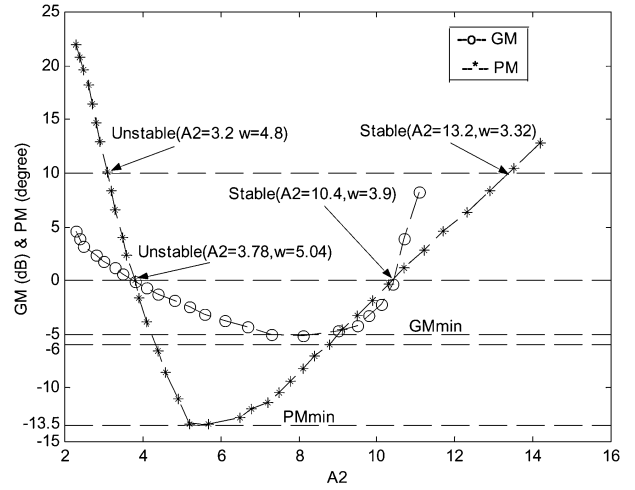

Fig. 14 The intersection points between M loci and boundaries of constant gain–phase margin with $K_p = 20$ and $T_n = 0.15$.

Substituting $s = j\omega$ into Eq. (38) and varying A_2 from 0 to ∞ enables a set of A_{2i} and K_i, related to ω_i, to be obtained directly from Eqs. (11–14). Alternatively, let $K = 0$ dB; Eq. (37) is rearranged as follows:

$$
\begin{aligned}
f(s) &= 34K_pN_1(A_1)K_g(s+4)(s^2+1.5s+4)(11.17s^3+21.98s^2 \\
&\quad + 1504.22s + 1180.8)\cos\theta + 34K_pN_1(A_1)K_g(s+4) \\
&\quad \times (s^2+1.5s+4)(11.17s^3+21.98s^2+1504.22s \\
&\quad + 1180.8)(-j)\sin\theta + (T_ns+1)(s^5+3.07s^4+252.36s^3 \\
&\quad + 375.28s^2+984s)\big[(s+4)(s+34)(s^2+1.5s+4) \\
&\quad + 76.5(s+0.8)(s+8)N_2(A_2)\big] \\
&= U\cdot\cos\theta + V\cdot\sin\theta + W = 0
\end{aligned}
\tag{39}
$$

Substituting $s = j\omega$ into Eq. (39) and varying A_2 from 0 to ∞ enables a set of A_{2i}, and θ_i related to ω_i, to be also obtained directly from Eqs. (16–19).

Based on the foregoing analysis, Fig. 13 plots the M_{GM} locus, the M_{PM} locus, and the boundaries of constant gain (K) and phase (θ). The stability boundary can be seen to intersect two M loci at two points, $L_1(0.17, 0.30)$ and $L_2(0.34, 0.77)$. Restated, two limit cycles are predicted: they are identical to those in Table 2 of Ref. 4. Figure 12 shows the characteristics of these two limit cycles.

Figure 14 plots the relationship between the gain–phase margins and the amplitude of the limit cycle. The case of $GM = PM = 0$ ($K = 0$ dB, $\theta = 0$ deg) was considered earlier. At $GM_{min} = -5$ dB and $PM_{min} = -13.5$ deg, according to Fig. 14, the system eliminates a limit cycle because Q_1 is in the limit-cycle region. Another two conditions are considered to determine the accuracy of Fig. 14. When K is decreased by 6 dB, the dashed line does not intersect the GM curve, implying that the system moved from a limit-cycle region into an asymptotically stable region. However, when θ is increased by 10 deg, the dashed line intersects the PM curve at two points, ($A_2 = 3.2$, $\omega = 4.8$) and ($A_2 = 13.2$, $\omega = 3.32$). Consequently, the system has two limit cycles, one of which is stable and the other of which is unstable. Figure 15 presents the time simulations under the preceding two conditions, and the results match those in Fig. 14.

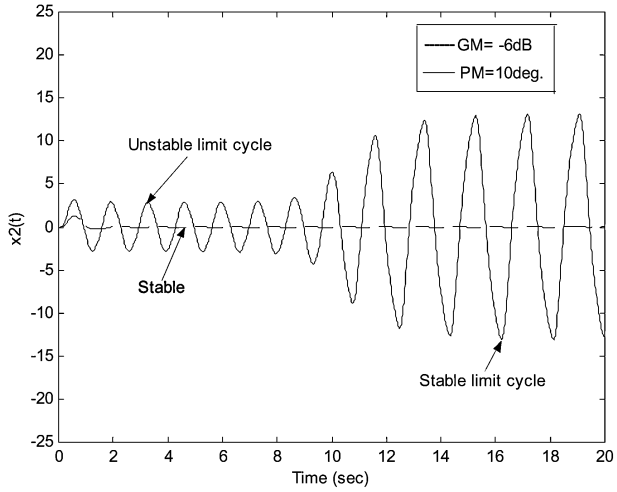

Fig. 15 Simulation results with decreased gain and increased phase.

V. Conclusions

This paper applies some effective methods, including one involving gain–phase margin tester technology, the M-locus method, and the parameter plane method, to analyze the limit cycle of PIOs. Both single and multiple nonlinearities in PIO systems are considered. A concise method is presented to determine the gain–phase margins and the M locus is plotted for limit-cycle analysis. The analysis of PIOs in the current literature should be modified according to computer simulations such that more information about limit cycles can be extracted by our approach.

Acknowledgments

This paper was supported by the R. O. C. Ministry of Education under Grant 91X104 EX-91-E-FA06-4-4. The authors acknowledge K. W. Han and Y. C. Chang for their guidance and suggestions.

References

[1]Matranga, G. J., "Analysis of X-15 Landing Approach and Flare Characteristics Determined from the First 30 Flights," NASA TN D-1057, July 1961.

[2]Smith, J. W., and Berry, D. T., "Analysis of Longitudinal Pilot-Induced Oscillation Tendencies of the YF-12 Aircraft," NASA TND-7900, Feb. 1975.

[3]Amato, F., Iervolino, R., Scala, S., and Verde, l., "Category II Pilot-in-the-Loop Oscillations Analysis from Robust Stability Methods," *Journal of Guidance, Control, and Dynamics*, Vol. 24, No. 3, 2001, pp. 531–538.

[4]Anderson, M. R., "Pilot-Induced Oscillations Involving Multiple Nonlinearities," *Journal of Guidance, Control, and Dynamics*, Vol. 21, No. 5, 1998, pp. 786–791.

[5]Klyde, D. H., McRuer, D. T., and Myers, T. T., "Pilot-Induced Oscillation Analysis and Predication with Actuator Rate Limiting," *Journal of Guidance, Control, and Dynamics*, Vol. 20, No. 1, 1997, pp. 81–89.

[6]Duda, H., "Prediction of Pilot-in-the-Loop Oscillations due to Rate Saturation," *Journal of Guidance, Control, and Dynamics*, Vol. 20, No. 3, 1997, pp. 581–587.

[7]Liebst, B. S., Chapa, M. J., and Leggett, D. B., "Nonlinear Prefilter to Prevent Pilot-Induced Oscillations due to Actuator Rate Limiting," *Journal of Guidance, Control, and Dynamics*, Vol. 25, No. 4, 2002, pp. 740–747.

[8]Gelb, A., and Vander Velde, W. E., *Multiple Input Describing Functions and Nonlinear System Design*, McGraw–Hill, New York, 1968, pp. 520–524.
[9]Han, K. W., *Nonlinear Control Systems—Some Practical Methods*, Academic Cultural Co., Santa Clara, CA, 1977, pp. 254–268.
[10]Han, K. W., and Thaler, G. J., "Control System Analysis and Design Using a Parameter Space Method," *IEEE Transactions on Automatic Control*, Vol. 11, No. 3, 1966, pp. 560–563.
[11]Ackermann, J., "Parameter Space Design of Robust Control Systems," *IEEE Transactions on Automatic Control*, Vol. 25, No. 6, 1980, pp. 1058–1072.
[12]Ackermann, J., Kaesbauer, D., and Muench, R., "Robust Gamma-Stability Analysis in a Plant Parameter Space," *Automatica*, Vol. 27, No. 1, 1991, pp. 75–85.
[13]Cavallo, A., Maria, G. E., and Verde, L., "Robust Control Systems: A Parameter Space Design," *Journal of Guidance, Control, and Dynamics*, Vol. 15, No. 5, 1992, pp. 1207–1215.
[14]Siljak, D. D., "Analysis and Synthesis of Feedback Control Systems in the Parameter Plane," *IEEE Transactions on Industry and Application*, Vol. 83, Nov. 1964, pp. 466–473.
[15]Siljak, D. D., "Parameter Space Methods for Robust Control Design: A Guide Tour," *IEEE Transactions on Automatic Control*, Vol. 34, No. 7, 1989, pp. 674–688.
[16]Siljak, D. D., *Nonlinear Systems—The Parameter Analysis and Design*, Wiley, New York, 1969, pp. 232–275.
[17]Chang, C. H., and Han, K. W., "Gain Margins and Phase Margins for Control Systems with Adjustable Parameters," *Journal of Guidance, Control, and Dynamics*, Vol. 13, No. 3, 1990, pp. 404–408.
[18]Shenton, A. T., and Shafiei, Z., "Relative Stability for Control Systems with Adjustable Parameters," *Journal of Guidance, Control, and Dynamics*, Vol. 17, No. 2, 1994, pp. 304–310.
[19]Chang, C. H., and Han, K. W., "Gain Margin and Phase Margin Analysis of a Nuclear Reactor Control System with Multiple Transport Lags," *IEEE Transactions on Nuclear Science*, Vol. 36, No. 4, 1989, pp. 1418–1425.
[20]Chang, C. H., and Chang, M. K., "Analysis of Gain Margins and Phase Margins of a Nonlinear Reactor Control System," *IEEE Transactions on Nuclear Science*, Vol. 41, No. 4, 1994, pp. 1686–1691.
[21]Chang, M. K., Chang, C. H., and Han, K. W., "Gain Margins and Phase Margins for Nonlinear Control Systems with Adjustable Parameters," *Proceedings of IEEE Industry Application Society Annual Meeting*, IEEE Publ., Piscataway, NJ, 1993, pp. 2123–2130.
[22]Chang, Y. C., and Han, K. W., "Analysis of Limit Cycles for a Low Flying Vehicle with Three Nonlinearities," *International Journal of Actual Problems of Aviation and Aerospace Systems, USSR*, Vol. 6, No. 2, 1998, pp. 38–50.
[23]Chang, Y. C., Liu, C. C., and Han, K. W., "Limit Cycle Analysis of a Helicopter Borne Gun-Turret Control System," *Proceedings of the AASRC/CIROC/CSCA Aerospace Joint Conference*, Aeronautical and Astronautical Society of the Republic of China, Taipei, PRC, 1999, pp. 1–6.
[24]Shenton, A. T., "Parameter Space Design of PID Limit Cycle Controllers," *Proceedings of the American Control Conference*, American Automatic Control Council, Evanston, IL, 1999, pp. 3342–3346.